CRYSTAL GROWTH & DESIGN

Article

Cite This: Cryst. Growth Des. 2020, 20, 713−722

pubs.acs.org/crystal

Polymorphism in Solid Dispersions

Karina Sanabria Ortiz,[†,‡] José R. Hernández Espinell,[†,‡] Desire Ortiz Torres,[†,‡] Vilmalí López-Mejías,[*,†,‡] and Torsten Stelzer[*,‡,§]

[†]Department of Chemistry, University of Puerto Rico, Río Piedras Campus, San Juan, Puerto Rico 00931, United States

[‡]Crystallization Design Institute, Molecular Sciences Research Center, University of Puerto Rico, San Juan, Puerto Rico 00926, United States

[§]Department of Pharmaceutical Sciences, University of Puerto Rico, Medical Sciences Campus, San Juan, Puerto Rico 00936, United States

Supporting Information

ABSTRACT: Solid dispersions embed active pharmaceutical ingredients in polymeric carriers to improve their solubility. Three solid dispersion preparation techniques are typically employed: solvent evaporation, solvent-fusion, and fusion methods. Although these are also widely recommended as preparative methods for phase diagram determination, few examples exist concerning their effect on the resulting polymorph, once the solid dispersion is produced. In this study, the influence of these methods on the polymorphic form obtained in crystalline solid dispersions (CSDs) composed of flufenamic acid (FFA) and polyethylene glycol was investigated. The physical mixtures and CSDs were characterized by powder X-ray diffraction, infrared spectroscopy, and differential scanning calorimetry. The results reveal that the fusion method leads to concomitant polymorphs (mainly FFA I and III) in the CSDs. In contrast, the solvent evaporation and solvent-fusion methods lead to FFA III. Collectively, these results demonstrate that preparative methods have a significant influence on the phase diagrams determined (average relative deviation ≤8%), which are often used to justify the design space of manufacturing processes, including those deemed "continuous." Consequently, choosing a preparation method that results in the desired polymorph is crucial to ensure accurate determination of phase diagrams and critical quality attributes of formulations.

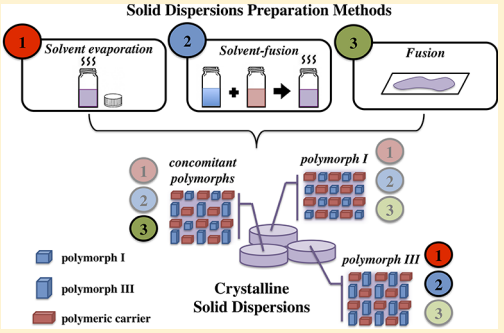

1. INTRODUCTION

Solid dispersions embed active pharmaceutical ingredients (APIs) in polymeric carriers to improve their solubility.[1−3] Generally, two types of solid dispersions can be distinguished with respect to the solid state of the API, namely, amorphous and crystalline.[2−4] On the one hand, amorphous solid dispersions can enhance the dissolution rate of poorly water-soluble APIs.[3−7] However, amorphous solids are thermodynamically unstable and tend to crystallize without control over the solid form, which alters the solubility and bioavailability of the final drug formulation.[2,8−11] On the other hand, recent studies have proven the feasibility to process crystalline solid dispersions (CSDs) in continuous manufacturing settings while still improving the dissolution of the API.[2,4,12,13] However, the application of CSDs is yet to be widespread, due to (i) the recent emergence of advanced formulation technologies (e.g., hot melt extrusion and additive manufacturing) for CSDs,[2,13−15] (ii) the contrastingly large interest in gaining insights into the stabilization of amorphous solid dispersions,[4,6] and last (iii) the lack of understanding about how the crystalline state behaves in dynamic environments encountered during manufacturing processes.[16]

Three main preparation techniques are typically reported for amorphous or crystalline solid dispersions: solvent evaporation, solvent-fusion, and fusion methods.[7,17−21] For the solvent evaporation method, both the API and the carrier are separately dissolved in a common solvent, which is evaporated, once the substances are mixed to produce a solid dispersion.[7,17−20] The API and the carrier must be soluble in the solvent employed.[17] The solvent-fusion method requires that the API is separately dissolved in a solvent and that the polymer is melted prior to mixing and further evaporation of the solvent to produce the solid dispersion.[18−20] It has been documented that the solvent-fusion method can lead to either homogeneous or heterogeneous mixtures prior to the solvent evaporation.[18,20] In the fusion method, the API and carrier are melted, and the mixture is then cooled at a specific rate to produce the solid dispersion.[7,17,19,20] An important prerequisite for this method is that the API and carrier must be miscible and thermally stable in the molten state while being processed.[17]

These three techniques are also widely recommended as preparation steps prior to phase diagram determination, which are often used to justify the design space of manufacturing

Received: August 27, 2019
Revised: December 6, 2019
Published: December 17, 2019

DOI: 10.1021/acs.cgd.9b01138
Cryst. Growth Des. 2020, 20, 713−722

processes.[22−25] However, very few examples exist in the literature concerning the effect of these methods on the resulting polymorph of the API in the CSDs obtained.[16,19,26] Polymorphism, a relatively common phenomena in pharmaceutical compounds, allows molecules to exhibit multiple crystalline phases and alters their physicochemical properties (e.g., solubility, bioavailability, melting point).[16,27] Gaining awareness of the impact of polymorphism when employing each of these solid dispersion preparation methods might lead to higher accuracy in the determination of phase diagrams and control over the quality attributes of APIs in CSDs.[25]

In this study, the influence of these preparation methods on the resulting polymorph in CSDs composed of flufenamic acid (FFA) and polyethylene glycol (PEG) was investigated. FFA is a nonsteroidal anti-inflammatory drug that presents a high degree of polymorphism;[28] however, only two forms (FFA I and III) are stable and readily accessible under ambient conditions.[16,28] These two polymorphs are enantiotropically related with FFA III being the stable form below 42 °C.[16,28] PEGs are commonly used to produce CSDs,[3,12,13,29−31] particularly for novel polymer-based formulation strategies in the realm of continuous manufacturing.[3,12,13,29−34]

CSDs starting with (10−80 wt %) FFA I or III in PEG were prepared by each of the aforementioned methods. The polymorphic purity of the resulting CSDs after each preparation method was determined by powder X-ray diffraction (PXRD) and Fourier transform infrared (FTIR) spectroscopy. Differential scanning calorimetry (DSC) was employed to determine the phase diagrams for the resulting CSDs. The binary eutectic phase diagrams derived from the CSDs were compared to phase diagrams produced from untreated physical mixtures (FFA I-PEG and FFA III-PEG). Moreover, phase diagrams were predicted applying the Lacoulonche model[35] to obtain qualitative information about the theoretical liquidus curve as well as eutectic temperature of the systems under study. The average relative deviation (ARD %) was calculated to assess the impact of polymorphism on the phase diagrams as a result of each of these preparation methods with respect to physical mixtures utilized as untreated controls. The results obtained serve to (i) guide the selection process for solid dispersion preparation methods, (ii) advocate for the use of characterization tools that ensure the accurate determination of the phase diagram for the polymorphic form of interest, and (iii) gain control over the critical quality attributes of CSDs (e.g., polymorph of the API).[36]

2. MATERIALS AND METHODS

2.1. Materials. FFA I (≥97%) and methanol (ACS reagent, ≥99.8%) were purchased from Sigma-Aldrich. Ethanol (200 proof) was procured from Pharmaco-Aaper. PEG (≤100%) with an average molecular weight of 10 000 g/mol and phosphorus(V) oxide (P_2O_5, ≥98%) were acquired from Alfa Aesar. All chemicals were used "as received" without further purification. FFA III was produced by recrystallization from a methanol solution as previously described in the literature.[16,37] For molecular structures of FFA as well as the packing motifs of selected FFA polymorphs see Supporting Information or search the Cambridge Structural Database.

2.2. Preparation of Solid Dispersions. *Physical Mixtures.* Physical mixtures were prepared as reported in the literature.[16] Briefly, desired amounts of PEG as well as FFA I or III (10−80 wt %) were ground using a mortar with pestle for 5 min at ambient conditions in the absence of solvent. Afterward, the physical mixtures were analyzed by PXRD (Supporting Information) to confirm that the energy input through grinding had no adverse effect on the polymorphic form prior to the solid dispersion preparation method and phase diagram determination by DSC.

Solvent Evaporation Method. The solvent evaporation method was employed as described in the literature.[7,18−21] Briefly, desired amounts of FFA (I or III) and PEG were separately dissolved in 20 mL scintillation vials by adding 5 mL of methanol or 10 mL of ethanol, depending on the solubility of FFA.[38−40] To ensure complete dissolution of FFA and PEG solutions were heated to 40 °C (VWR Digital 2 block heater 120). After 1 h, the clear solutions were filtered through a Fisher Scientific poly(tetrafluoroethylene) (PTFE) membrane syringe filter (25 mm, 0.2 μm pore size) to eliminate the presence, if any, of particulate impurities or possible FFA seed crystals (≥0.2 μm) that could influence the crystallization. To exclude this as a possible impact, CSDs were prepared starting with FFA I and III, respectively. The undersaturated solutions with respect to FFA were both transferred into a new 20 mL vial, resulting in mixtures containing FFA and PEG in the desired composition. Afterward, the solvent was removed employing a fast or slow evaporation method.

For fast evaporation rate (faster generation of supersaturation), reduced pressure was employed for 40 min using a Rotavapor R-210 from Büchi Labortechnik AG with recirculating chiller F-105, heating bath B-491, vacuum pump V-700, and vacuum controller V-850 at 40 °C (122 mbar and 38 mbar for methanol and ethanol, respectively). For slow evaporation rate (slower generation of supersaturation), the vials were covered with perforated aluminum foil at 40 °C in a heating block for 3 (methanol) to 7 d (ethanol). The resulting CSDs were stored in a desiccator at ambient temperature under 0% humidity using P_2O_5 for 2−4 d before further solid-state characterization was performed. CSDs of FFA-PEG system have been shown to be stable for ≥900 d.[16] Every composition was prepared and characterized in duplicate.

Solvent-Fusion Method. The solvent-fusion method was employed as previously described in the literature.[18−20] Briefly, desired amounts of PEG were weighted into a 20 mL scintillation vial and melted at 69 °C for 10 min using a heating block. The amount of FFA needed to achieve the desired compositions (10−80 wt % in PEG) was dissolved and filtered into the vials containing the molten PEG, as described in the solvent evaporation method. Afterward, the mixtures were homogenized for 10 s with alternate movements in a Vortex mixer (VWR Vortexer mini 120 V). The solvent was then evaporated under reduced pressure from the mixture as described in the solvent evaporation method. The resulting CSDs were stored as described above before further solid-state characterization was conducted. Every composition was prepared and characterized in duplicate.

Fusion Method. This method was conducted as previously reported in the literature,[17,19] using a hot stage (Linkam Scientific Instruments Ltd., LTS 420) coupled with a polarized light microscope (Nikon Eclipse LV100N POL). The physical mixtures (∼60 mg) were evenly distributed onto a microscope slide and equilibrated at 20 °C prior to heating (5 °C/min) to 150 °C. Afterward, the molten mixtures were cooled to 25 °C at a rate of 20 or 2 °C/min, for fast- and slow-cooling profiles, respectively. The thermal stability of both FFA and PEG under these conditions has been discussed in previous work.[16] The hot stage was calibrated measuring the melting point of water. Optical micrographs were recorded using a Nikon DS-Fi2 camera and NIS Elements BR software version 4.30.01. Once the CSDs were obtained, the microscope slides were stored in a desiccator as described above before further solid-state characterization was conducted. Every composition was prepared and characterized in triplicate.

2.3. Solid-State Characterization. Prior to the characterization of the CSDs, the samples were carefully transferred and gently ground using a mortar with pestle for 5 min at ambient conditions in the absence of solvent. Preliminary PXRD analysis confirmed that no polymorphic phase transformation was induced through the increased energy input, which is consistent with previously reported literature.[16]

Powder X-ray Diffraction (PXRD) Analysis. PXRDs were collected for each CSD at 300 K in a Rigaku XtalLAB SuperNova microfocus X-ray diffractometer, with a Cu Kα radiation (λ = 1.5417 Å, 50 kV and 1 mA) source equipped with a HyPix3000 X-ray detector in

DOI: 10.1021/acs.cgd.9b01138
Cryst. Growth Des. 2020, 20, 713−722

transmission mode. Powders were affixed in MiTeGen microloops. Powder diffractograms were collected over an angular 2θ range of 5−40° (step size of 0.01°) using the fast phi experiment (120 s exposure). Data were analyzed in CrysAlis^{Pro} software version 1.171.3920a.

Samples obtained employing the fusion method that started with FFA I were characterized by PXRD at ambient condition employing a Bruker D8 Discover micro-diffractometer equipped with the General Area Detector Diffraction System (GADDS) and the VÅNTEC-2000 two-dimensional (2D) detector. The X-ray beam was made monochromatic with a graphite crystal (λ Cu Kα radiation = 1.541 78 Å, 40 kV and 40 mA). The powders were loaded in Kapton capillaries (0.8 mm) and mounted in a horizontal configuration on a sample stage affixed to a five-circle Eulerian cradle. The 2D diffraction data collection was controlled by the GADDS software. Two scans with rotation of the capillary were acquired with equal incident angle (θ_1) and detector angle (θ_2) at 5 and 40°, respectively. Diffraction patterns were obtained by integrating the 2D PXRD data using XRD2EVAL in the Bruker PILOT software (version 2014.11-0).

Differential Scanning Calorimetry (DSC). DSC analysis in a TA Q2000 equipped with a single-stage refrigeration system (RCS40) and calibrated with a standard (indium). Samples (~3.0000 ± 0.0001 mg) were weighed using an XP26 (Mettler Toledo) microbalance (±0.002 mg) and placed in aluminum pans that were hermetically sealed. The samples were equilibrated at 25 °C for 10 min before heating to 150 °C at 5 °C/min (±0.1 °C) under N_2 atmosphere (50 mL/min). The eutectic temperature and melting points of the liquidus curve were determined as peak temperatures during the first heating cycle using the TA Universal Analysis software version 4.5A. To construct the experimental phase diagrams the DSC measurements were conducted in duplicate.

Samples obtained employing the fusion method that started with FFA I were analyzed following the same heating profile as described above in a PerkinElmer DSC 8000 equipped with an Intracooler II. The calibration of the instrument was made with a standard (indium).

Fourier Transform Infrared Spectroscopy (FTIR). FTIR spectra were collected using a Bruker Tensor-27 attenuated total reflectance spectrometer between 400 and 4000 cm^{-1} with a resolution of 4 cm^{-1} averaging 32 scans (1 scan/s). The data were collected with the OPUS Data Collection Program version 7.2.

For samples employing the fusion method with FFA I the FTIR spectra were collected using a Nicolet 6700 FTIR attenuated total reflectance spectrometer (Thermo Scientific) between 400 and 4000 cm^{-1} with a resolution of 4 cm^{-1} averaging 64 scans (1 scan/s) using the Omnic 8.3 software version.[41]

2.4. Thermodynamic Modeling. The thermodynamic model developed by Lacoulonche et al.[35] has been successfully applied to predict phase diagrams of various API-polymer systems[35,42−44] using known values of physicochemical properties for the pure components.[35,45,46] The Lacoulonche model was derived for binary systems applying the Flory−Huggins lattice theory[47] for polymer solutions, which assumes that the substance and the polymer are not miscible in the solid state.[35] In this model, for the compositions below the eutectic ($\phi_s < \phi_{eut}$), the liquidus temperature ($T_{\phi s<\phi eut}$) can be calculated using Equation 1, while above the eutectic composition ($\phi_s > \phi_{eut}$), the liquidus temperature ($T_{\phi s>\phi eut}$) can be calculated using Equation 2.[42]

$$T_{\phi_s<\phi_{eut}} = \frac{\Delta H_{f,s} + \Delta W_{s,p}(1-\phi_s)^2}{\frac{\Delta H_{f,s}}{T_{m,s}} - R\left[\ln(\phi_s) + (1-\phi_s)\left(1 - \frac{V_{m,s}}{V_{m,p}}\right)\right]} \quad (1)$$

$$T_{\phi_s>\phi_{eut}} = \frac{\Delta H_{f,p} + \Delta W_{s,p}(\phi_s)^2}{\frac{\Delta H_{f,p}}{T_{m,p}} - R\left[\ln(1-\phi_s) + (\phi_s)\left(1 - \frac{V_{m,p}}{V_{m,s}}\right)\right]} \quad (2)$$

Parameters employed in Equations 1 and (2) include the universal gas constant R (8.314 4598 J/mol·K), volume fraction ϕ_s (−), heat of fusion $\Delta H_{f,s}$ and $\Delta H_{f,p}$ (J/mol), melting point $T_{m,s}$ and $T_{m,p}$ (K), and molar volume $V_{m,s}$ and $V_{m,p}$ (cm^3/mol) for each substance (s) and polymer (p), respectively. The total interaction energy per macromolecular volume element between the substance and the polymer, $\Delta W_{s,p}$ (J/mol) in Equations 1 and (2) was set to zero ($\Delta W_{s,p} = 0$), with the assumption that the mixing of the compounds is athermal.[42,43] The molar volume (V_m) for component i (substance or polymer) can be calculated using Equation 3, where M is the molecular weight (g/mol) and ρ (g/cm^3) is the density for compound i.

$$V_{m,i} = \frac{M_i}{\rho_i} \quad (3)$$

The density of PEG and FFA I is 1.20 and 1.47 g/cm^3, respectively, as reported in the literature.[28,48] The density of FFA III (ρ = 1.501 g/cm^3) is not readily available in the literature and was calculated using Equation 4, where M is the molecular weight of FFA (g/mol), N_A is the Avogadro's number (6.022 140 86 × 10^{23} mol^{-1}), Z is the number of formula units for FFA III, and V is the cell volume for FFA III (cm^3).[28] The parameters needed for Equation 4 were extracted from the crystallographic information file (CIF file, Reference Code = FPAMCA) obtained from the Cambridge Structural Database.[28,49] Other parameters needed for the thermodynamic modeling are summarized in the Supporting Information.

$$\rho = \frac{Z \cdot M}{V \cdot N_A} \quad (4)$$

The volume fraction (ϕ_s) can be calculated applying Equation 5, where ρ_s and ρ_p (g/cm^3) are the densities of the substance (s) and polymer (p), respectively, and x_s is the weight fraction of the substance.

$$\phi_s = \frac{1}{1 + \frac{x_s \cdot \rho_p}{(1-x_s)\rho_s}} \quad (5)$$

Average Relative Deviation (ARD%). To assess the impact of the preparation method on the phase diagram with respect to untreated physical mixtures of known polymorphic purity, the ARD% for the liquidus line above the eutectic composition, the FFA side, was calculated using Equation 6.

$$\text{ARD\%} = \frac{100}{N}\sum_{i=1}^{N}\left|\frac{T_{m,i}^{MIX} - T_{m,i}^{CSD}}{T_{m,i}^{MIX}}\right| \quad (6)$$

In Equation 6 N is the total number of experimental values, and $T_{m,i}^{MIX}$ and $T_{m,i}^{CSD}$ are the melting temperatures (°C) of the physical mixtures and the CSDs, respectively, at a given composition calculated from the best possible fit of basic polynomial and exponential functions. All trend lines of the liquidus curves demonstrate a relatively good coefficient of determination (R^2) with at least $R^2 \geq 0.95$. The ARD% values are summarized in the Supporting Information.

3. RESULTS AND DISCUSSION

3.1. Solvent Evaporation Method. The solvent evaporation method relies on the dissolution of the initial polymorph (FFA I or III), then supersaturation is generated as a result of the evaporation of the solvent, and the thermodynamics and kinetics of the system drive the crystallization process.[25,50,51] For the solvent evaporation method, the solvents (methanol or ethanol) were removed by employing a fast or slow evaporation rate at a constant temperature, 40 °C (2 °C below the transition temperature, where FFA III is stable).[37,40,52,53] These parameters were selected based on previous accounts reporting the selective crystallization of either FFA I or III from methanol or ethanol depending on the supersaturation.[28,37,40] Generally, quick cooling or solvent evaporation leads to high supersaturation levels, which often

DOI: 10.1021/acs.cgd.9b01138
Cryst. Growth Des. 2020, 20, 713−722

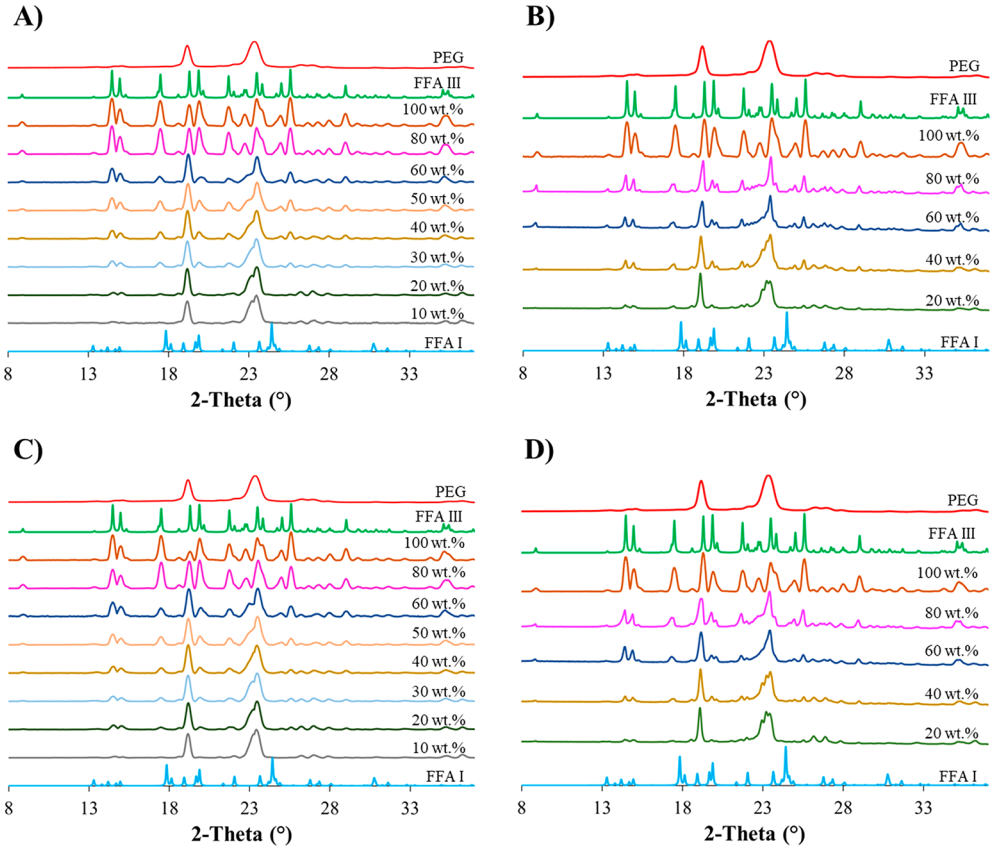

Figure 1. PXRD for CSDs obtained by the solvent evaporation method in methanol using a fast (A, B) and slow (C, D) evaporation rate at 40 °C starting with FFA III (A, C) or FFA I (B, D). Simulated PXRD of FFA I (Reference Code = FPAMCA11, blue),[28] experimental PXRDs of treated CSDs (various colors), simulated PXRD of FFA III (Reference Code = FPAMCA, green),[49] and experimental PXRD of PEG (red). Simulated PXRDs were extracted from the crystallographic information files (CIF files) obtained from the Cambridge Structural Database.

favors the formation of metastable polymorphs compared to slower rates.[54,55] However, this was not the case for the FFA-PEG system. After employing both evaporation rates, using either of the two solvents, CSDs of FFA III were obtained in every composition (Figure 1). Thus, if the intention is to prepare a CSD containing FFA I, the commercial form, then this preparation method might not be suitable as shown in Figure 1.

The solvent evaporation method was also conducted using a slow evaporation rate at a constant temperature, 60 °C (18 °C above the transition temperature, where FFA III is metastable).[37,40,52,53] One would expect that, under these conditions, this preparative method would lead to CSDs containing FFA I. However, the PXRD analysis confirms that all CSDs resulted in FFA III for every composition (Supporting Information). Similar crystallization behavior of FFA was observed by Vázquez et al.[40] by employing cooling crystallization to slowly generate supersaturation of FFA in various alcohols in the temperature range from 5 to 60 °C. The authors also reported that FFA III was consistently obtained, even at temperatures above the transition point (42 °C).[37,40,52,53] Thus, both crystallization processes (evaporation and cooling from methanol and ethanol) seem to favor the FFA III even when combined with PEG and irrespective of whether the process temperature is above or below the transition temperature of the enantiotropically related polymorphic pair. This suggests an important role of the solvent in guiding the formation of FFA III.

The binary eutectic phase diagrams of the resulting CSDs obtained by the solvent evaporation method at 40 °C were experimentally derived using DSC and compared to the physical mixtures of FFA III-PEG and the predicted Lacoulonche model (Figure 2). The physical mixtures of FFA III-PEG are chosen as the control, because this polymorph is obtained at every composition when employing this method (Figure 1). Moreover, the Lacoulonche model provides an approximation of the thermodynamic behavior for the eutectic phase diagram. The liquidus curve of the phase diagrams determined using CSDs prepared by the solvent evaporation method show good agreement with both the model and the physical mixtures. The latter is demonstrated by the low ARD% values (≤5) for all solvents and evaporation rates employed. It is worth mentioning that the CSDs prepared starting with FFA I by the solvent evaporation method (orange squares, Figure 2) and analyzed by DSC correspond to CSDs of FFA III as discussed above. Therefore, the phase diagrams shown in Figure 2, "CSD starting with FFA I", are representative of CSDs containing FFA III and not FFA I. This is further reinforced when these phase diagrams are contrasted to those determined for "CSD starting with FFA III", the FFA III-PEG physical mixtures, or predicted by the Lacoulonche model for FFA III. The phase diagrams produced by the CSDs obtained through the solvent evaporation method at 60 °C are available in the Supporting Information and provide similar results.

3.2. Solvent-Fusion Method. For the solvent-fusion method, the solvents (methanol and ethanol) employed to

DOI: 10.1021/acs.cgd.9b01138
Cryst. Growth Des. 2020, 20, 713−722

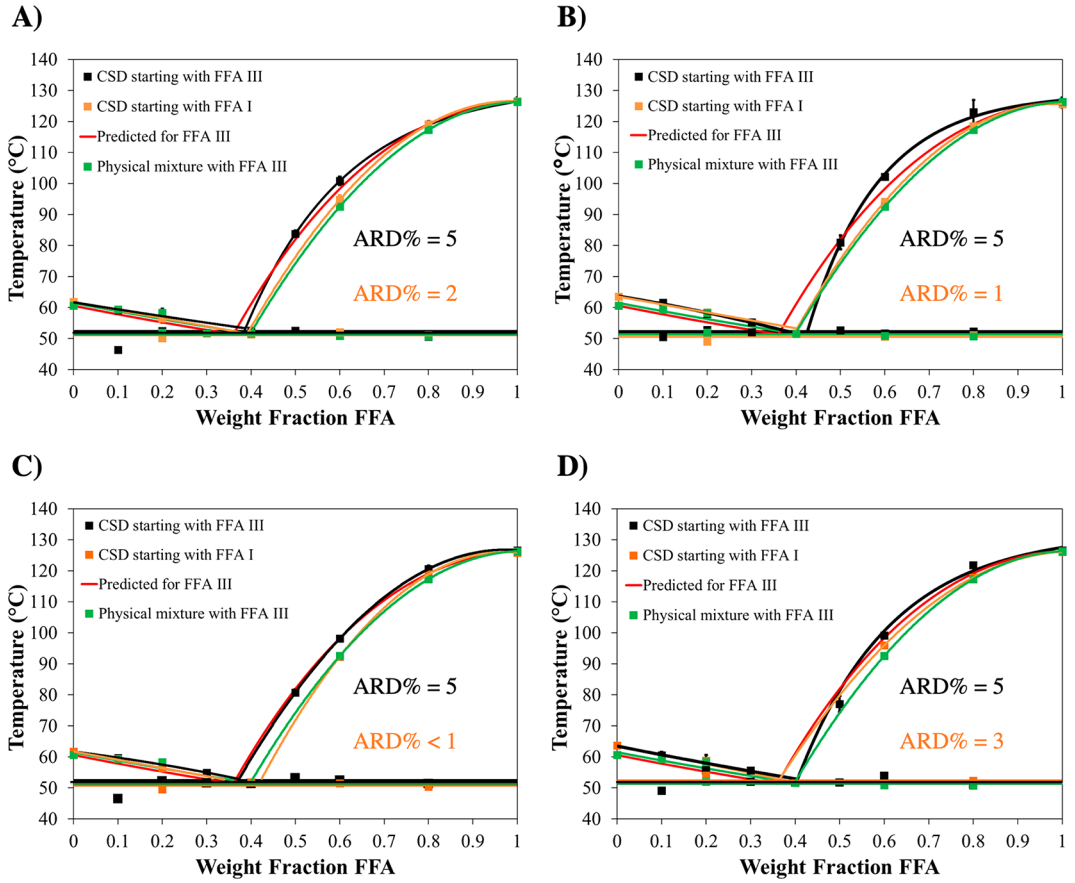

Figure 2. Phase diagrams of CSDs obtained by the solvent evaporation method at 40 °C starting with FFA III (black) or FFA I (orange) using fast (A, C) and slow (B, D) evaporation rates in methanol (A, B) or ethanol (C, D) compared to the predicted Lacoulonche model for FFA III-PEG (red) and the FFA III-PEG physical mixture (green). If error bars cannot be noticed, these are obstructed by the data points.

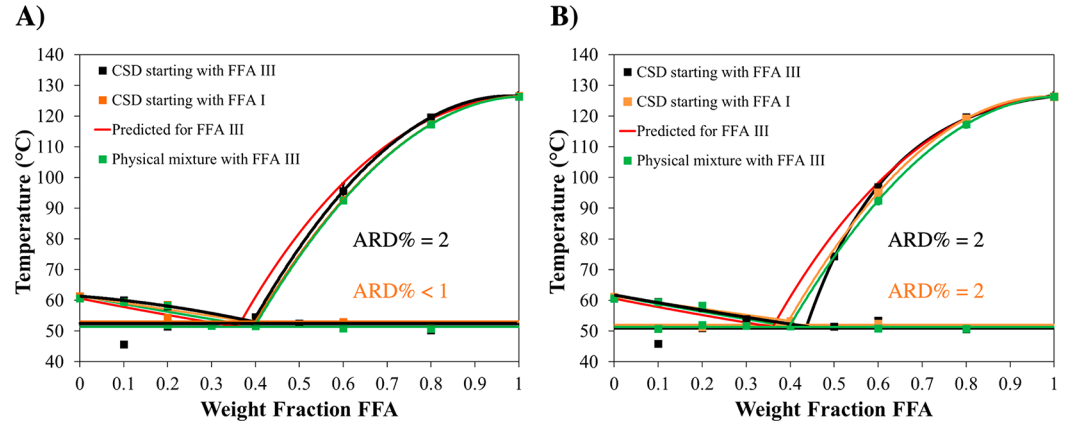

Figure 3. Phase diagrams of CSDs obtained by the solvent-fusion method starting with FFA III (black) or FFA I (orange) using (A) methanol and (B) ethanol compared to the predicted Lacoulonche model for FFA III-PEG (red) and the FFA III−PEG physical mixtures (green). If error bars cannot be noticed, these are obstructed by the data points.

dissolve the FFA were removed under reduced pressure at a constant temperature of 40 °C after they mixed with the molten PEG. The CSDs obtained were identified as FFA III for every composition (Supporting Information). These results agree with those obtained when the solvent evaporation method is used. As in the solvent evaporation method, the initial polymorph (FFA I or III) is completely dissolved when undergoing this solvent-fusion method. Thus, once supersaturation is reached, the polymorphic outcome is dictated by the thermodynamics and kinetics of the system,[25,50,51] which is similar to the solvent evaporation method, leading to the formation of FFA III in the CSDs. Therefore, if the CSD should contain the commercial form, FFA I, this preparation method will also not be suitable. The similarity in the results of both preparation methods presented here as well as those reported by Vázquez et al.[40] for cooling crystallization supports the critical role of the solvent (particularly alcohols) in guiding the formation of FFA III despite the presence of PEG in the solution.

DOI: 10.1021/acs.cgd.9b01138
Cryst. Growth Des. 2020, 20, 713−722

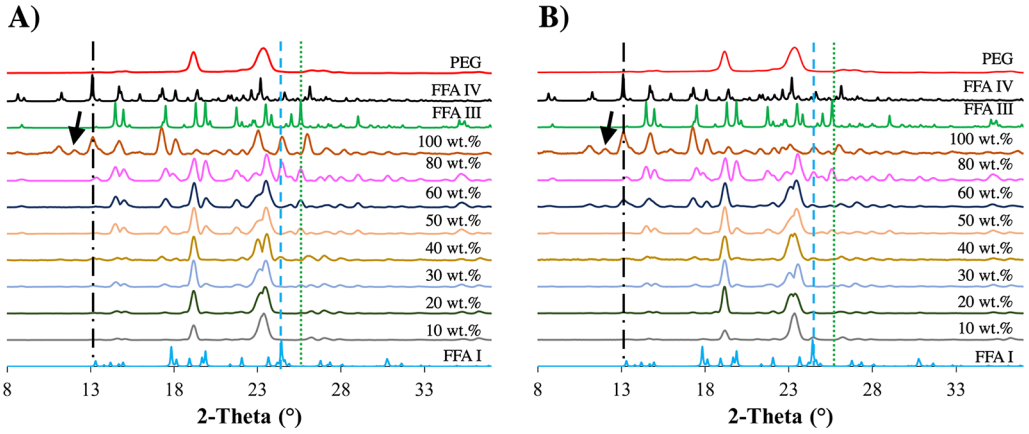

Figure 4. PXRDs for CSDs obtained by the fusion method using (A) fast- and (B) slow-cooling process starting with FFA III. Simulated PXRD of FFA I (Reference Code = FPAMCA11, blue),[28] experimental PXRD of treated CSDs (various colors), simulated PXRD of FFA III (Reference Code = FPAMCA, green),[49] simulated PXRD of FFA IV (Reference Code = FPAMCA15 black),[28] and experimental PXRD of PEG (red). Blue dashed line, the green dotted line, and broken black line correspond to the characteristic peaks of FFA I, III, and IV, respectively. Black arrow indicates a peak at 11.8° in 2θ that corresponds to FFA IX.[28] Simulated PXRDs were extracted from the crystallographic information files (CIF files) obtained from the Cambridge Structural Database.

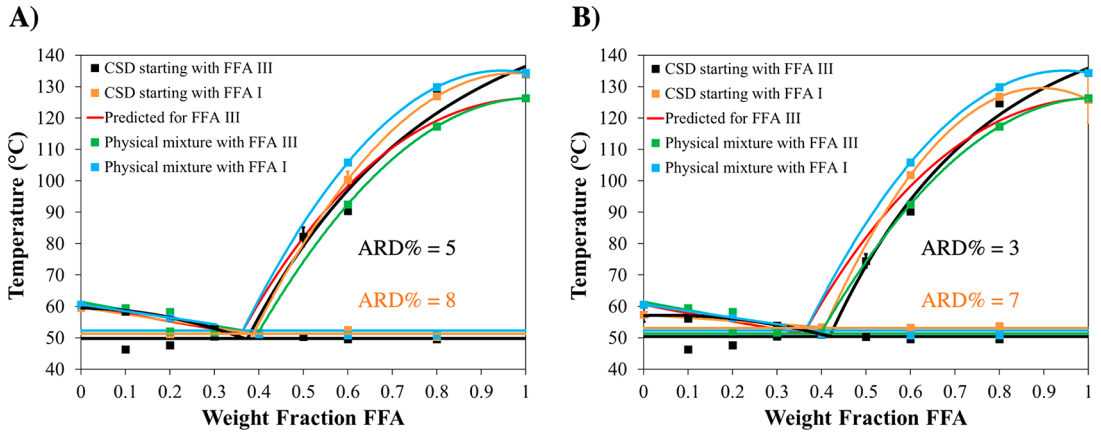

Figure 5. Phase diagrams of CSDs obtained by the fusion method starting with FFA III (black) or FFA I (orange) using (A) fast- and (B) slow-cooling process compared to the predicted Lacoulonche model for FFA III-PEG (red), the physical mixtures of FFA III−PEG (green), and FFA I−PEG (blue). If error bars cannot be noticed, these are obstructed by the data points. ARD% shown are calculated with respect to FFA III-PEG physical mixture. The values for FFA I-PEG are summarized in the Supporting Information.

The phase diagrams of the CSDs prepared by the solvent-fusion method were compared with those obtained using FFA III-PEG physical mixtures and the Lacoulonche model. As in the solvent evaporation method, the physical mixtures of FFA III-PEG are chosen as the control, because FFA III is obtained at every composition (Figure 3). In Figure 3 it can be seen that the liquidus curves of the phase diagrams determined using CSDs prepared by the solvent-fusion method are in good agreement with the Lacoulonche model and the physical mixtures (ARD% $\leq$ 2). CSDs produced starting with FFA I with the solvent-fusion method (orange squares, Figure 3) and further analyzed by DSC correspond also to FFA III. For this reason, the phase diagrams shown in Figure 3 (independent if started with FFA I or III) are representative of CSDs containing FFA III and not FFA I.

3.3. Fusion Method. For the fusion method, physical mixtures were prepared and melted before different cooling rates (fast or slow) were applied. The resulting CSDs were analyzed by PXRD; those prepared starting with FFA III are illustrated in Figure 4, while CSDs prepared starting with FFA I are shown in the Supporting Information. Unlike the previous two methods, the solid-state analysis of the CSDs generated by the fusion method reveals that most CSDs present a mixture of various FFA polymorphs, mainly FFA I and III. In those cases where concomitant polymorphism[54,55] was not observed, the predominant form was FFA III. On this account, this preparation method is not suitable to produce CSDs containing either of the two polymorphs in pure form.

In recent years, various studies have shown that melt crystallization enables the access to previously unexplored polymorphic forms and more readily leads to the appearance of concomitant polymorphs compared to solution crystallization.[56−62] However, the mechanism leading to the generation of polymorphs (single phase or concomitantly) in melt crystallization processes is poorly understood. More so in cases where there is additional complexity due to the presence of a second component such as polymers. In terms of the FFA-PEG system, the crystallization of the supercooled melt occurs within a very broad temperature range (20−119 °C) showing the uncontrolled (stochastic) nature of the process. The presence of competing thermodynamic and kinetic (nucleation, growth, phase transformation) factors[54,55] due to the

DOI: 10.1021/acs.cgd.9b01138
Cryst. Growth Des. 2020, 20, 713−722

generation of various supercooled regions within the melt (spatial randomness)[63] might trigger the nucleation of multiple forms of FFA. Moreover, the molecular mobility might also be reduced in melts compared to solutions leading to suppressed kinetics, which might be further altered through the presence of the polymer.[10,62,64] However, quick molecular mobility is essential to permit the diffusion and surface phenomena[10] that are needed for nucleation, crystal growth, and solvent (melt)-mediated phase transformation processes.[16,65,66] Specifically for the FFA-PEG system, we observed that, as the amount of PEG increases, the supercooling (driving force)[25,51] at which nucleation occurs decreases during the melt crystallization process (Supporting Information). Thus, we suspect that, in the presence of the polymer PEG, highly metastable forms (e.g., FFA IV and IX)[28] do not readily form or are not able to grow into mature crystals that can be detected by the solid-state characterization techniques employed in this study.

However, when the fusion method was applied for the pure API (100 wt % FFA I or III), traces of highly metastable polymorphic forms of FFA (FFA IV and in some cases FFA IX) in addition to FFA I and III were obtained when employing either of the cooling rates (Figure 4 and Supporting Information).[28] These results reinforce our suggestion that the presence of the polymer, in this study PEG, inhibits the formation of highly metastable forms of FFA in the CSDs. Overall, these findings suggests that, contrary to when polymers are used as a heteronucleants,[28,67−71] the addition of polymers during melt crystallization might hinder kinetic processes (nucleation, growth, phase transformation) that promote highly metastable forms and favor thermodynamically more stable forms instead. This might be an important consideration when developing CSDs through polymer-based formulations strategies (e.g., hot melt extrusion or additive manufacturing) for CSDs,[2,13−15] in continuous manufacturing settings.

The phase diagrams of the CSDs prepared by the fusion method were compared with those obtained from physical mixtures of both polymorphs with PEG and the Lacoulonche model of FFA III (Figure 5). For the discussion of the fusion method physical mixtures containing FFA I and III in PEG are both employed as controls, because the characterization revealed the presence of concomitant polymorphs.[54,55] Figure 5 shows that the DSC data and liquidus curves (trend lines) of the CSDs obtained through this method do not show a consistent thermodynamic behavior, which confirms the presence of a mixture of FFA polymorphs (Figure 5). Moreover, the liquidus curves obtained above the eutectic composition are significantly altered and varies between the liquidus curves obtained from physical mixtures of FFA I and III in PEG, respectively. These findings are supported by relatively large ARD% values (≤8). Similar ARD% values (≤8) were also obtained with respect to FFA I-PEG physical mixtures (Supporting Information). Thus, for this polymorphic compound, and possibly many others, the fusion method leads to the inaccurate determination of the binary eutectic phase diagram in PEG. Moreover, further physicochemical properties such as dissolution rate are also likely to be affected.[72−74]

4. CONCLUSIONS

The appearance of different polymorphs as result of different CSDs preparation methods has been shown to significantly alter the resulting phase diagram (ARD% ≤ 8). Therefore, the solid state needs to be carefully characterized prior to DSC measurements after these preparation methods are employed. Alternatively, untreated physical mixtures may be used to generate phase diagrams, because they present a relatively accurate thermodynamic behavior and prevent issues associated with concomitant polymorphs or appearance of undesired polymorphs. On this account, when the employed compounds are prone to polymorphism, choosing a solid dispersion preparation method that results in the desired polymorphic form is crucial to ensure accurate determination of the phase diagram and quality attributes of the CSDs.

■ ASSOCIATED CONTENT

Supporting Information

The Supporting Information is available free of charge at https://pubs.acs.org/doi/10.1021/acs.cgd.9b01138.

Thermodynamic modeling parameters, details regarding molecular structures of FFA and PEG, the packing motifs of selected FFA polymorphs, the characterization of the physical mixtures, and resulting CSDs prepared by each of the three methods employing PXRD and FTIR, as well as additional phase diagrams, summary of ARD%, and the supercooling obtained in the fusion method (PDF)

■ AUTHOR INFORMATION

Corresponding Authors

*E-mail: vilmali.lopez@upr.edu. (V.L.-M.)
*E-mail: torsten.stelzer@upr.edu. (T.S.)

ORCID

Vilmalí López-Mejías: 0000-0003-2138-8414
Torsten Stelzer: 0000-0003-3881-0183

Author Contributions

K.S.O. and J.R.H.E. contributed equally to this work.

Funding

The initial development of this work occurred at the New York University's Materials Research Science and Engineering Center (NYU-MRSEC), while participating at the NSF-funded NYU-MRSEC's Student-Faculty Summer Program (DMR-1420073). The primary support was provided by the Puerto Rico Science, Technology & Research Trust under Award Nos. 2016-00081 and 2016-00082 and the Institutional Research Funds (FIPI Funds) of the University of Puerto Rico, Río Piedras Campus. Infrastructure support was provided in part by the National Institute on Minority Health and Health Disparities (8G12MD007600). The Bruker AXS D8 DISCOVER GADDS X-ray micro-diffractometer was acquired through the Chemistry Research Instrumentation and Facilities (CRIF) Program (CHE-0840277), and the PerkinElmer DSC 8000 was acquired through the NYU-MRSEC (DMR-0820341). The Rigaku XtalLAB SuperNova single-crystal X-ray micro-diffractometer was acquired through the Major Research Instrumentation Program (CHE-1626103). The authors gratefully acknowledge the Research Initiative for Scientific Enhancement (RISE) Program under Grant No. 5R25GM061151-14 and the Puerto Rico Louis Stokes Alliance for Minority Participation (PR-LSAMP, HRD-1400868) for personnel and material support. Further development of this work occurred under the NSF-funded Wisconsin - Puerto Rico Partnership for Research and Education in Materials (DMR-1827894).

DOI: 10.1021/acs.cgd.9b01138
Cryst. Growth Des. 2020, 20, 713−722

Notes

The authors declare no competing financial interest.

■ ACKNOWLEDGMENTS

The authors acknowledge F. M. Reyes Figueroa and G. López Burgos, both members of the Crystallization Design Institute, for their contributions to the PXRD and DSC data collection, analysis, and interpretation. The authors also acknowledge the training and assistance provided by Dr. T. Hu during the PXRD experiments performed at NYU. Finally, the authors thank Drs. M. D. Ward, B. Kahr, L. Yu and their research groups for insightful conversations regarding this project.

■ REFERENCES

(1) Ye, X.; Patil, H.; Feng, X.; Tiwari, R. V.; Lu, J.; Gryczke, A.; Kolter, K.; Langley, N.; Majumdar, S.; Neupane, D.; et al. Conjugation of Hot-Melt Extrusion with High-Pressure Homogenization: A Novel Method of Continuously Preparing Nanocrystal Solid Dispersions. *AAPS PharmSciTech* **2016**, *17* (1), 78−88.

(2) Desai, P. M.; Hogan, R. C.; Brancazio, D.; Puri, V.; Jensen, K. D.; Chun, J. H.; Myerson, A. S.; Trout, B. L. Integrated Hot-Melt Extrusion − Injection Molding Continuous Tablet Manufacturing Platform: Effects of Critical Process Parameters and Formulation Attributes on Product Robustness and Dimensional Stability. *Int. J. Pharm.* **2017**, *531* (1), 332−342.

(3) Shah, S.; Maddineni, S.; Lu, J.; Repka, M. A. Melt Extrusion with Poorly Soluble Drugs. *Int. J. Pharm.* **2013**, *453* (1), 233−252.

(4) Baghel, S.; Cathcart, H.; O'Reilly, N. J. Polymeric Amorphous Solid Dispersions: A Review of Amorphization, Crystallization, Stabilization, Solid-State Characterization, and Aqueous Solubilization of Biopharmaceutical Classification System Class II Drugs. *J. Pharm. Sci.* **2016**, *105* (9), 2527−2544.

(5) Maniruzzaman, M.; Nair, A.; Scoutaris, N.; Bradley, M. S. A.; Snowden, M. J.; Douroumis, D. One-Step Continuous Extrusion Process for the Manufacturing of Solid Dispersions. *Int. J. Pharm.* **2015**, *496* (1), 42−51.

(6) Tian, Y.; Jones, D. S.; Andrews, G. P. An Investigation into the Role of Polymeric Carriers on Crystal Growth within Amorphous Solid Dispersion Systems. *Mol. Pharmaceutics* **2015**, *12* (4), 1180−1192.

(7) Nikghalb, L. A.; Singh, G.; Singh, G.; Kahkeshan, K. F. Solid Dispersion: Methods and Polymers to Increase the Solubility of Poorly Soluble. *Drugs. J. Appl. Pharm. Sci.* **2012**, *2* (10), 170−175.

(8) Burcham, C. L.; Florence, A. J.; Johnson, M. D. Continuous Manufacturing in Pharmaceutical Process Development and Manufacturing. *Annu. Rev. Chem. Biomol. Eng.* **2018**, *9* (1), 253−281.

(9) Thommes, M.; Ely, D. R.; Carvajal, M. T.; Pinal, R. Improvement of the Dissolution Rate of Poorly Soluble Drugs by Solid Crystal Suspensions. *Mol. Pharmaceutics* **2011**, *8* (3), 727−735.

(10) Janssens, S.; Van den Mooter, G. Review: Physical Chemistry of Solid Dispersions. *J. Pharm. Pharmacol.* **2009**, *61* (12), 1571−1586.

(11) Censi, R.; Gigliobianco, M. R.; Casadidio, C.; Di Martino, P. Hot Melt Extrusion: Highlighting Physicochemical Factors to Be Investigated While Designing and Optimizing a Hot Melt Extrusion Process. *Pharmaceutics* **2018**, *10* (3), 89.

(12) Hwang, I.; Kang, C.-Y.; Park, J.-B. Advances in Hot-Melt Extrusion Technology toward Pharmaceutical Objectives. *J. Pharm. Invest.* **2017**, *47* (2), 123−132.

(13) Mascia, S.; Heider, P. L.; Zhang, H.; Lakerveld, R.; Benyahia, B.; Barton, P. I.; Braatz, R. D.; Cooney, C. L.; Evans, J. M. B.; Jamison, T. F.; et al. End-to-End Continuous Manufacturing of Pharmaceuticals: Integrated Synthesis, Purification, and Final Dosage Formation. *Angew. Chem., Int. Ed.* **2013**, *52* (47), 12359−12363.

(14) Goole, J.; Amighi, K. 3D Printing in Pharmaceutics: A New Tool for Designing Customized Drug Delivery Systems. *Int. J. Pharm.* **2016**, *499* (1), 376−394.

(15) Prasad, E.; Islam, M. T.; Goodwin, D. J.; Megarry, A. J.; Halbert, G. W.; Florence, A. J.; Robertson, J. Development of a Hot-Melt Extrusion (HME) Process to Produce Drug Loaded Affinisol 15LV Filaments for Fused Filament Fabrication (FFF) 3D Printing. *Addit. Manuf.* **2019**, *29*, 100776.

(16) Hernández Espinell, J. R.; López-Mejías, V.; Stelzer, T. Revealing Polymorphic Phase Transformations in Polymer-Based Hot Melt Extrusion Processes. *Cryst. Growth Des.* **2018**, *18* (4), 1995−2002.

(17) Eloy, J. O.; Marchetti, J. M. Solid Dispersions Containing Ursolic Acid in Poloxamer 407 and PEG 6000: A Comparative Study of Fusion and Solvent Methods. *Powder Technol.* **2014**, *253*, 98−106.

(18) Chiou, W. L.; Riegelman, S. Pharmaceutical Applications of Solid Dispersion Systems. *J. Pharm. Sci.* **1971**, *60* (9), 1281−1302.

(19) Martínez-Oharriz, M. C.; Martín, C.; Goñi, M. M.; Rodríguez-Espinosa, C.; Tros-Ilarduya, M. C.; Zornoza, A. Influence of Polyethylene Glycol 4000 on the Polymorphic Forms of Diflunisal. *Eur. J. Pharm. Sci.* **1999**, *8* (2), 127−132.

(20) Mogal, S. A.; Gurjar, P. N.; Yamgar, D. S.; Kamod, A. C. Solid Dispersion Technique for Improving Solubility of Some Poorly Soluble. *Drugs. Der Pharm. Lett.* **2012**, *4* (5), 1574−1586.

(21) Shete, S.; Gadhave, V.; Gaikwad, D. Enhancement of Solubility and Dissolution Rate of Simvastatin by Ternary Solid Dispersion Technique. *J. Pharm. Sci. Innovation* **2015**, *3* (5), 36−41.

(22) Tian, Y.; Booth, J.; Meehan, E.; Jones, D. S.; Li, S.; Andrews, G. P. Construction of Drug-Polymer Thermodynamic Phase Diagrams Using Flory-Huggins Interaction Theory: Identifying the Relevance of Temperature and Drug Weight Fraction to Phase Separation within Solid Dispersions. *Mol. Pharmaceutics* **2013**, *10*, 236−248.

(23) Yu, L. X.; Lionberger, R. A.; Raw, A. S.; D'Costa, R.; Wu, H.; Hussain, A. S. Applications of Process Analytical Technology to Crystallization Processes. *Adv. Drug Delivery Rev.* **2004**, *56* (3), 349−369.

(24) Black, J. T.; Kohser, R. A. *Degarmo's Materials and Processes in Manufacturing,* 11th ed.; Jonh Wiley and Sons, Inc.: Danvers, MA, 2012.

(25) Beckmann, W. *Crystallization: Basic Concepts and Industrial Applications;* Wiley-VCH Verlag GmbH & Co. KGaA: Weinheim, Germany, 2013.

(26) Höhne, G. W. H.; Hemminger, W. F.; Flammersheim, H.-J. *Differential Scanning Calorimetry,* 2nd ed.; Springer-Verlag: Berlin, Germany, 2003.

(27) Hamaed, H.; Pawlowski, J. M.; Cooper, B. F. T.; Fu, R.; Eichhorn, S. H.; Schurko, R. W. Application of Solid-State 35Cl NMR to the Structural Characterization of Hydrochloride Pharmaceuticals and Their Polymorphs. *J. Am. Chem. Soc.* **2008**, *130* (33), 11056−11065.

(28) López-Mejías, V.; Kampf, J. W.; Matzger, A. J. Nonamorphism in Flufenamic Acid and a New Record for a Polymorphic Compound with Solved Structures. *J. Am. Chem. Soc.* **2012**, *134* (24), 9872−9875.

(29) Içten, E.; Giridhar, A.; Taylor, L. S.; Nagy, Z. K.; Reklaitis, G. V. Dropwise Additive Manufacturing of Pharmaceutical Products for Melt-Based Dosage Forms. *J. Pharm. Sci.* **2015**, *104* (5), 1641−1649.

(30) Park, J. B.; Kang, C. Y.; Kang, W. S.; Choi, H. G.; Han, H. K.; Lee, B. J. New Investigation of Distribution Imaging and Content Uniformity of Very Low Dose Drugs Using Hot-Melt Extrusion Method. *Int. J. Pharm.* **2013**, *458* (2), 245−253.

(31) Dierickx, L.; Saerens, L.; Almeida, A.; De Beer, T.; Remon, J. P.; Vervaet, C. Co-Extrusion as Manufacturing Technique for Fixed-Dose Combination Mini-Matrices. *Eur. J. Pharm. Biopharm.* **2012**, *81* (3), 683−689.

(32) Tiwari, R. V.; Patil, H.; Repka, M. A. Contribution of Hot-Melt Extrusion Technology to Advance Drug Delivery in the 21st Century. *Expert Opin. Drug Delivery* **2016**, *13* (3), 451−464.

(33) Stanković, M.; Frijlink, H. W.; Hinrichs, W. L. J. Polymeric Formulations for Drug Release Prepared by Hot Melt Extrusion: Application and Characterization. *Drug Discovery Today* **2015**, *20* (7), 812−823.

DOI: 10.1021/acs.cgd.9b01138
Cryst. Growth Des. 2020, 20, 713−722

(34) Vasconcelos, T.; Sarmento, B.; Costa, P. Solid Dispersions as Strategy to Improve Oral Bioavailability of Poor Water Soluble Drugs. *Drug Discovery Today* **2007**, *12* (23−24), 1068−1075.
(35) Lacoulonche, F.; Chauvet, a.; Masse, J. An Investigation of Flurbiprofen Polymorphism by Thermoanalytical and Spectroscopic Methods and a Study of Its Interactions with Poly-(Ethylene Glycol) 6000 by Differential Scanning Calorimetry and Modelling. *Int. J. Pharm.* **1997**, *153* (2), 167−179.
(36) Yu, L. X.; Amidon, G.; Khan, M. A.; Hoag, S. W.; Polli, J.; Raju, G. K.; Woodcock, J. Understanding Pharmaceutical Quality by Design. *AAPS J.* **2014**, *16* (4), 771−783.
(37) Gilpin, R. K.; Zhou, W. Infrared Studies of the Polymorphic States of the Fenamates. *J. Pharm. Biomed. Anal.* **2005**, *37* (3), 509−515.
(38) Domańska, U.; Pobudkowska, A.; Pelczarska, A. Solubility of Sparingly Soluble Drug Derivatives of Anthranilic Acid. *J. Phys. Chem. B* **2011**, *115* (11), 2547−2554.
(39) Alshehri, S.; Shakeel, F. Solubility Measurement, Thermodynamics and Molecular Interactions of Flufenamic Acid in Different Neat Solvents. *J. Mol. Liq.* **2017**, *240*, 447−453.
(40) Vázquez Marrero, V. R.; Piñero Berríos, C.; De Dios Rodríguez, L.; Stelzer, T.; López-Mejías, V. In the Context of Polymorphism: Accurate Measurement, and Validation of Solubility Data. *Cryst. Growth Des.* **2019**, *19* (7), 4101−4108.
(41) Maulvi, F. A.; Dalwadi, S. J.; Thakkar, V. T.; Soni, T. G.; Gohel, M. C.; Gandhi, T. R. Improvement of Dissolution Rate of Aceclofenac by Solid Dispersion Technique. *Powder Technol.* **2011**, *207* (1−3), 47−54.
(42) Vippagunta, S.; Wang, Z.; Hornung, S.; Krill, S. L. Factors Affecting the Formation of Eutectic Solid Dispersions and Their Dissolution Behavior. *J. Pharm. Sci.* **2007**, *96* (2), 294−304.
(43) Baird, J. A.; Taylor, L. S. Evaluation and Modeling of the Eutectic Composition of Various Drug-Polyethylene Glycol Solid Dispersions. *Pharm. Dev. Technol.* **2011**, *16* (3), 201−211.
(44) Lacoulonche, F.; Masse, J.; Chauvet, A.; Garcia, M. L.; Egea, M. A. An Investigation of FB Interactions with Poly(Ethylene Glycol) 6000, Poly(Ethylene Glycol) 4000, and Poly-∈-Caprolactone by Thermoanalytical and Spectroscopic Methods and Modeling. *J. Pharm. Sci.* **1998**, *87* (5), 543−551.
(45) Law, D.; Wang, W.; Schmitt, E. a; Long, M. a. Prediction of Poly(Ethylene) Glycol-Drug Eutectic Compositions Using an Index Based on the van't Hoff Equation. *Pharm. Res.* **2002**, *19* (3), 315−321.
(46) Prudic, A.; Ji, Y.; Sadowski, G. Thermodynamic Phase Behavior of API/Polymer Solid Dispersions. *Mol. Pharmaceutics* **2014**, *11* (7), 2294−2304.
(47) Flory, P. J. Thermodynamics of High Polymer Solutions. *J. Chem. Phys.* **1942**, *10* (1), 51−61.
(48) Polyethylene Glycol [MAK Value Documentation, 1998]. In *The MAK-Collection for Occupational Health and Safety;* Wiley-VCH Verlag GmbH & Co. KGaA, 2002; Vol. 10, pp 247−270. DOI: 10.1007/978-1-4419-6247-8_9074.
(49) Krishna Murthy, H. M.; Bhat, T. N.; Vijayan, M. Structure of a New Crystal Form of 2-{[3-(Trifluoromethyl)Phenyl]Amino}benzoic Acid (Flufenamic Acid). *Acta Crystallogr., Sect. B: Struct. Crystallogr. Cryst. Chem.* **1982**, *B38*, 315−317.
(50) Papageorgiou, G.; Bikiaris, D.; Karavas, E.; Politis, S.; Docoslis, A.; Park, Y.; Stergiou, A.; Georgarakis, E. Effect of Physical State and Particle Size Distribution on Dissolution Enhancement of Nimodipine/PEG Solid Dispersions Prepared by Melt Mixing and Solvent Evaporation. *AAPS J.* **2006**, *8*, E623−31.
(51) Myerson, A. S.; Erdemir, D.; Lee, A. Y. *Handbook of Industrial Crystallization,* 3rd ed.; Cambridge University Press: Cambridge, UK, 2019. DOI: 10.1017/9781139026949.
(52) Hu, Y.; Liang, J. K.; Myerson, A. S.; Taylor, L. S. Crystallization Monitoring by Raman Spectroscopy: Simultaneous Measurement of Desupersaturation Profile and Polymorphic Form in Flufenamic Acid Systems. *Ind. Eng. Chem. Res.* **2005**, *44* (5), 1233−1240.
(53) Hu, Y.; Wikström, H.; Byrn, S. R.; Taylor, L. S. Estimation of the Transition Temperature for an Enantiotropic Polymorphic System from the Transformation Kinetics Monitored Using Raman Spectroscopy. *J. Pharm. Biomed. Anal.* **2007**, *45* (4), 546−551.
(54) Bernstein, J.; Davey, R. J.; Henck, J.-O. Concomitant Polymorphs. *Angew. Chem., Int. Ed.* **1999**, *38*, 3440−3461.
(55) Lee, I. S.; Lee, A. Y.; Myerson, A. S. Concomitant Polymorphism in Confined Environment. *Pharm. Res.* **2008**, *25* (4), 960−968.
(56) Chen, S.; Guzei, I.; Yu, L. New Polymorphs of ROY and New Record for Coexisting Polymorphs of Solved Structures. *J. Am. Chem. Soc.* **2005**, *127* (27), 9881−9885.
(57) Zhu, Q.; Shtukenberg, A. G.; Carter, D. J.; Yu, T.-Q.; Yang, J.; Chen, M.; Raiteri, P.; Oganov, A. R.; Pokroy, B.; Polishchuk, I.; et al. Resorcinol Crystallization from the Melt: A New Ambient Phase and New "Riddles. *J. Am. Chem. Soc.* **2016**, *138* (14), 4881−4889.
(58) Yang, J.; Hu, C. T.; Zhu, X.; Zhu, Q.; Ward, M. D.; Kahr, B. DDT Polymorphism and the Lethality of Crystal Forms. *Angew. Chem.* **2017**, *129* (34), 10299−10303.
(59) Shtukenberg, A.; Freundenthal, J.; Gunn, E.; Yu, L.; Kahr, B. Glass-Crystal Growth Mode for Testosterone Propionate. *Cryst. Growth Des.* **2011**, *11* (10), 4458−4462.
(60) Shtukenberg, A. G.; Hu, C. T.; Zhu, Q.; Schmidt, M. U.; Xu, W.; Tan, M.; Kahr, B. The Third Ambient Aspirin Polymorph. *Cryst. Growth Des.* **2017**, *17*, 3562−3566.
(61) Shtukenberg, A. G.; Zhu, Q.; Carter, D. J.; Vogt, L.; Hoja, J.; Schneider, E.; Song, H.; Pokroy, B.; Polishchuk, I.; Tkatchenko, A.; et al. Powder Diffraction and Crystal Structure Prediction Identify Four New Coumarin Polymorphs. *Chem. Sci.* **2017**, *8* (7), 4926−4940.
(62) Shtukenberg, A. G.; Tan, M.; Vogt-Maranto, L.; Chan, E. J.; Xu, W.; Yang, J.; Tuckerman, M. E.; Hu, C. T.; Kahr, B. Melt Crystallization for Paracetamol Polymorphism. *Cryst. Growth Des.* **2019**, *19* (7), 4070.
(63) van Gerven, T.; Stankiewicz, A. Structure, Energy, Synergy, Time − The Fundamentals of Process Intensification. *Ind. Eng. Chem. Res.* **2009**, *48* (5), 2465−2474.
(64) Zhang, S.; Britten, J. F.; Chow, A. H. L.; Lee, T. W. Y. Impact of Crystal Structure and Polymer Excipients on the Melt Crystallization Kinetics of Itraconazole Polymorphs. *Cryst. Growth Des.* **2017**, *17* (6), 3433−3442.
(65) Cardew, P. T.; Davey, R. J. The Kinetcs of Solvent-Mediated Phase Transformations. *Proc. R. Soc. London, Ser. A* **1985**, *398* (1815), 415−428.
(66) Davey, R. J.; Cardew, P. T.; McEwan, D.; Sadler, D. E. Rate Controlling Processes in Solvent-Mediated Phase Transformations. *J. Cryst. Growth* **1986**, *79* (1-3), 648−653.
(67) Curcio, E.; López-Mejías, V.; Di Profio, G.; Fontananova, E.; Drioli, E.; Trout, B. L.; Myerson, A. S. Regulating Nucleation Kinetics through Molecular Interactions at the Polymer-Solute Interface. *Cryst. Growth Des.* **2014**, *14* (2), 678−686.
(68) López-Mejías, V.; Kampf, J. W.; Matzger, A. J. Polymer-Induced Heteronucleation of Tolfenamic Acid: Structural Investigation of a Pentamorph. *J. Am. Chem. Soc.* **2009**, *131* (13), 4554−4555.
(69) McClelland, A. A.; López-Mejías, V.; Matzger, A. J.; Chen, Z. Peering at a Buried Polymer-Crystal Interface: Probing Heterogeneous Nucleation by Sum Frequency Generation Vibrational Spectroscopy. *Langmuir* **2011**, *27* (6), 2162−2165.
(70) Lopez-Mejías, V.; Knight, J. L.; Brooks, C. L.; Matzger, A. J. On the Mechanism of Crystalline Polymorph Selection by Polymer Heteronuclei. *Langmuir* **2011**, *27* (12), 7575−7579.
(71) López-Mejías, V.; Myerson, A. S.; Trout, B. L. Geometric Design of Heterogeneous Nucleation Sites on Biocompatible Surfaces. *Cryst. Growth Des.* **2013**, *13* (8), 3835−3841.
(72) Hilfiker, R. *Polymorphism;* Wiley-VCH Verlag GmbH & Co.: Weinheim, Germany, 2006.
(73) Brittain, H. G. *Polymorphism in Pharmaceutical Solids,* 2nd ed.; Informa Healthcare, USA, Inc.: New York, 2009. DOI: 10.1016/S0168-3659(01)00252-8.

DOI: 10.1021/acs.cgd.9b01138
Cryst. Growth Des. 2020, 20, 713−722

(74) Bernstein, J. *Polymorphism in Molecular Crystals;* Oxford University Press: Oxford, UK, 2002. DOI: 10.1093/acprof:oso/9780199236565.001.0001.

DOI: 10.1021/acs.cgd.9b01138
Cryst. Growth Des. 2020, 20, 713−722